


Magnetically Guided Intracartilaginous Delivery of Kartogenin Improves Stem Cell-Targeted Degenerative Arthritis Therapy

Zengxin Jiang^{1,*}, Zeng Zhang^{1,*}, Shuo Li^{2,*}, Sen Lin³, Hengfeng Yuan¹ 

¹Department of Orthopaedics, Shanghai Jiaotong University Affiliated Sixth People's Hospital, Shanghai, People's Republic of China; ²Department of Joint Bone Disease Surgery, Changhai Hospital, Second Military Medical University, Shanghai, People's Republic of China; ³National Engineering Research Center, East China University of Science and Technology, Shanghai, People's Republic of China

*These authors contributed equally to this work

Correspondence: Sen Lin; Hengfeng Yuan, Email linsen@ecust.edu.cn; yuanhf@shsmu.edu.cn

Background: Degenerative joint disease or osteoarthritis (OA) is a leading cause of disability worldwide. Intra-articular injection is the mainstay nonsurgical treatment for OA. However, dense cartilage and a lack of vasculature often limit the ability of drugs to reach cell or tissue targets at the concentrations necessary to elicit the desired biological response. Kartogenin (KGN), a small molecular compound, possesses a strong capacity to promote chondrogenic differentiation of mesenchymal stem cells (MSCs). However, the rapid clearance of KGN from the intra-articular cavity limits its feasibility.

Materials and Methods: We constructed a magnetically guided biodegradable nanocarrier system (MNP) which enabled intracartilaginous delivery of KGN to promote chondrogenic differentiation by MSCs embedded within the articular matrix. Moreover, in preclinical models of OA, KGN-loaded MNPs exhibited increased tissue penetration and retention within the joint matrix under external magnetic guidance.

Results: Histological examination showed that compared with KGN alone, KGN-loaded MNPs enhanced chondrogenic differentiation and improved the structural integrity of both articular cartilage and subchondral bone.

Conclusion: This study demonstrates a practical method for intracartilaginous delivery using engineered nanocarriers, thus providing a new strategy to improve the efficacy of molecular therapeutic agents in the treatment of OA.

Keywords: osteoarthritis, kartogenin, magnetic nanoparticles, intracartilaginous

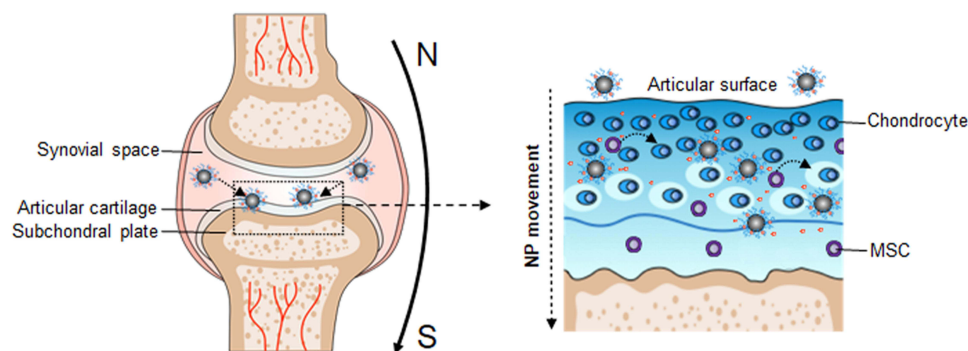
Introduction

Articular cartilage degeneration is considered to be the characteristic feature of osteoarthritis (OA).¹ Unfortunately, damaged cartilage has a limited capacity for self-repair and regeneration due to tissues that are believed to be avascular, alymphatic, and aneural.² Mesenchymal stem cells (MSCs) have previously been identified in healthy and diseased cartilage and are capable of self-renewal and differentiation into chondrocytes.^{3,4} Hence, it is likely that taking advantage of MSCs to regenerate cartilage will attenuate the progression of OA.

Recently, the small molecular compound, kartogenin (KGN, M=317.34), was reported to promote the differentiation of MSCs into chondrocytes through the CBF β -RUNX1 transcriptional program.⁵ However, the concentrations of KGN administered intraarticularly necessary for efficacy in vivo were much greater than those noted in in vitro studies. Although direct intra-articular injection of drugs can minimize adverse systemic side effects, the efficacy remains inadequate given that the small compounds are being rapidly cleared from the joint via lymphatics and subsynovial capillaries.⁶⁻⁹ Hence, there is an urgent need for effective drug delivery systems with local and safe administration of low doses.

Various intra-articular drug-delivery systems have been developed for OA treatment, including hydrogels, liposomes, micelles, dendrimers, exosomes and microspheres.^{10,11} The cartilage matrix is composed of a dense network of collagen

Graphical Abstract



fibrils with an approximate pore size of 60–200 nm and aggrecan proteoglycans.¹² Large carrier particles, such as nanocrystal-polymer particles, hyaluronic acid hydrogel, and chitosan, have prolonged residence times given their large size and aggregating properties, which prevent drugs from rapidly leaving the joint space. Nevertheless, these approaches do not always provide sufficient drug penetration into articular cartilage, which limits the effective drug concentration.^{13–15} Therefore, ideal drug carriers should overcome the size paradox by being small enough to penetrate into the cartilage but somehow not being rapidly cleared from the joint space.

MNPs have the characteristics of a large surface area, small particle size and superparamagnetic properties. Over the years, MNPs have gained increased attention and their therapeutic potential in applications geared toward diagnosis and targeted drug delivery.^{16,17} Magnetic nanoparticles play an important role for drug delivery in, for example, cancer diagnosis and therapy.^{18–21} To our knowledge, the literature contains few reports of iron oxide nanoparticles primed for magnetic targeting in OA treatment. Hence, in the present study, we aimed to explore the feasibility and effectiveness of magnetic iron oxide nanoparticles for the delivery of KGN into MSCs in joints. KGN-loaded magnetic nanoparticles (KGN-MNPs) were synthesized by using polylactide (PLA) to encapsulate KGN on the iron oxide nanoparticle surface. Magnetic iron oxide nanoparticles exhibit numerous advantages: small size, high specific surface area, excellent biocompatibility, superparamagnetic property and low toxicity.²² In addition, PLA is a polymer with excellent biocompatibility and biodegradability. PLA can be hydrolyzed *in vivo* into lactic acid, which is a natural midbody in glucose metabolism.²³ KGN-MNPs were injected into the joint cavity. Application of an external magnetic field to the joint prolonged KGN residency and promoted more KGN-MNPs to penetrate into cartilage. This study investigated the hypothesis that KGN-MNPs could be retained and obtained by more MSCs using a magnetic delivery method, and this KGN-based release strategy could efficiently and persistently promote chondrogenesis and attenuate OA progression.

Materials and Methods

The Synthesis and Characterization of MNPs and MNPs-KGN

MNPs

Iron oxide nanoparticles were synthesized according to previous studies.^{24,25} Briefly, 10 mmol $\text{FeCl}_3 \cdot 6\text{H}_2\text{O}$ (Cat No. 236,489, Sigma-Aldrich) and 0.6 mmol $\text{FeCl}_2 \cdot 4\text{H}_2\text{O}$ (Cat No. 44,939, Sigma-Aldrich) were dissolved in 25 mL deionized water. Then, the solution was mixed with 1.5 mL oleic acid (Cat No. O1008, Sigma-Aldrich) and 10 mL cyclohexane (Cat No. 227048, Sigma-Aldrich) with 0.25 mol/L NaOH (Cat No. S5881, Sigma-Aldrich) under vigorous stirring conditions for 30 min. Finally, the as-synthesized MNP nanoparticles were collected using a 0.6 T permanent magnet from the suspension and washed repeatedly with ethanol to eliminate the residues.

MNPs-KGN

A total of 100 mg of prepared MNPs nanoparticles was dispersed in 10 mL dichloromethane (Cat No. 270,997, Sigma-Aldrich), and used to dissolve 100 mg of poly (D,L-lactide acid, Cat No. 805,734, Sigma-Aldrich) and 15 mg KGN (Cat No. M4863, Abmole, Houston, TX, USA), to obtain KGN-loaded MNPs nanoparticles. The organic dispersion was evaporated under reduced pressure after emulsification by sonication on ice. MNPs-KGN nanoparticles were washed twice by magnetic decantation, lyophilized and stored at -80°C before use.

KGN Encapsulation Efficacy and Loading

The KGN concentrations in solutions were determined before (total amount) and after (free amount) centrifugation at 5000 rp for 10 min. The KGN encapsulation efficacy and KGN loading into the MNPs were calculated based on the following equations:

$\text{KGN encapsulation efficacy} = \text{wt KGN (total - free)}/\text{wt KGN total};$

$\text{KGN loading} = \text{wt KGN (total - free)}/\text{wt nanoparticles used for dosing}.$

Ex vitro Release Kinetics

The release studies were conducted with 20 mg/mL MNPs-KGN nanoparticles in phosphate buffered saline (PBS, Gibco; Thermo Fisher Scientific, Inc., Carlsbad, CA, USA) solution under vibration at 37°C . At given sampling intervals, the PBS solution was separated with MNPs-KGN nanoparticles and collected to detect the KGN concentration. Then, the same volume of PBS solution was added to mix with the residual MNPs-KGN nanoparticles for the next sampling time. The cumulative release profiles were evaluated to confirm the release kinetics of KGN.

Characterization of MNPs and MNPs-KGN

The Fourier-transform infrared (FTIR) spectra of MNPs and MNP-KGN were recorded on an FTIR spectrometer (Nicoletis 10, Thermo Scientific, USA) with samples in KBr pellets and a resolution of 4 cm^{-1} in the $4000\text{--}400\text{ cm}^{-1}$ region at 25°C . X-ray diffraction (XRD) patterns were determined using an X-ray power diffractometer (D8, BRUKER, Germany) with a copper anode generating Cu K α radiation ($\lambda=1.54\text{ \AA}$) at a scanning speed (2 θ) of $0.5^{\circ}/\text{min}$. Thermogravimetry (TG) analysis for MNPs and MNPs-KGN nanoparticles was conducted on a thermogravimetric apparatus (Q600SDT, TA, US) with temperatures ranging from room temperature to 650°C and a heating rate of $5^{\circ}\text{C}/\text{min}$ under N $_2$ protection. A droplet of 0.1 g/L MNPs or MNP-KGN suspension was dripped on a copper carbon grid and dried to observe the morphology by transmission electron microscopy (TEM) performed on an electron microscope (Ultra Plus, ZEISS, Germany) with an accelerating voltage of 100 kV. The agglomeration size distribution at 25°C was measured by dynamic light scattering (DLS) measurements using a commercial light-scattering setup ALV light-scattering instrument (ALV, Langen, Germany) and He-Ne lasers (22 mW) with wavelengths of 632.8 nm. To detect the isoelectric point (pI) value, a 10 mg sample was dispersed in 100 mL deionized water with ultrasonication for 1 h and the zeta potentials of the suspension were confirmed on a zeta potentiometer (Zetasizer Nano ZSP, Malvern, UK) at different pH values, which were adjusted by adding 0.05 mol/L HCl or NaOH solution. Then, the curve of potential against pH value was plotted to determine the pH value where the zeta potential was zero, which was taken as the pI value. The magnetic properties of the samples were measured using a vibrating sample magnetometer (730T, Lakeshore, USA) at 25°C . The iron concentrations of the tissue digestion solution were analyzed by an inductively coupled plasma-atomic emission spectrometry (ICP-AES) instrument (IRIS, ThermoElemental, USA) with a power of 1.3 kW and a plasma gas flow of 15 L/min. The KGN concentrations in solutions were determined using a high-performance liquid chromatograph (HPLC) (LC-20AT, Shimadzu, Japan) equipped with a C18 reverse-phase column (250 mm \times 4.6 mm i.d., particle size 5 μm) with a mobile phase of acetonitrile/water (v/v, 35/65) plus 0.1% formic acid.

In vitro Study of KGN-MNPs on MSCs

Cell Culture

Mesenchymal stem cells (MSCs) were isolated from the bone marrow of Sprague-Dawley rats as described previously.^{26,27} MSCs were cultured in regular growth medium consisting of low-glucose DMEM (Gibco) supplemented with 10% fetal bovine serum (FBS) (Gibco), 100 U/mL penicillin, and 100 $\mu\text{g}/\text{mL}$ streptomycin. All cultures were

maintained in an atmosphere of 5% CO₂ and 95% air at 37 °C. The experiments were performed using MSCs from the third to seventh passage.

Cell Viability and Differentiation

Cell viability was evaluated by the Cell Counting Kit-8 (CCK-8) assay (Beyotime, Shanghai, China). The cells were incubated with KGN-MNPs for 6 to 72 h, and the absorbance was measured using a spectrophotometric reader (SpectraMax 384, US) at 450 nm. To initiate chondrogenesis in primary MSCs, the cells were cultured in special chondrogenic induction medium (Cyagen, Guangzhou, China) as a positive control. The negative control was induction medium without TGF- β . For the KGN involved groups, the medium was replaced with DMEM containing a commensurable amount of KGN (100 nM).

Intracellular Uptake of KGN-MNPs

A magnet with 0.6 T strength was placed underneath the cell culture plate to serve as a magnetic dragging force. The intracellular uptake of KGN-MNPs was determined by Prussian blue staining (Servicebio, Wuhan, China). The cells were incubated with Prussian blue solution containing potassium ferrocyanide and hydrochloric acid for 60 min, and then with nuclear fast red solution for 2 min at 37 °C. The iron (Fe) concentration in MSCs was quantified using an inductively coupled plasma-atomic emission spectrometry instrument (IRIS, Thermo Elemental, US). The samples were prepared as follows: the cells were collected and washed thoroughly, and then heated to 70 °C for 24 h. Then, each sample was added to 1 mL of 37% HCl and reheated again to 70 °C for 12 hours. Finally, each sample was added to 3 mL of 2% nitric acid and filtered to remove any trace remaining organic matter and impurities. 4) Chondrocyte-specific Gene Expression in MSCs: Cells were treated with KGN-MNPs at the indicated concentration (KGN amount= 100 nM) for 72 h in serum-free DMEM. The RNA was extracted using an RNeasy kit (Qiagen), and cDNA was synthesized using SuperScript III reverse transcriptase (Invitrogen). The levels of specific genes were determined using TaqMan gene expression assays.

In vivo Study of KGN-MNPs in ACLT Models

Study Design

Male Sprague Dawley rats at 3 months of age were anesthetized with ketamine and xylazine. Medial arthrotomy was performed, followed by anterior cruciate ligament transection (ACLT) of the right knee as described previously.^{28,29} The sham group rats underwent medial arthrotomy only, and the intra-articular capsule was intact. On weeks 1, 3, 5, and 7, the rats were administered IA injections with KGN-MNPs (corresponding to 100 nM KGN) in 50 μ L of saline. Rats from the sham group received 50 μ L of saline. Regarding the magnet treatment group, the knees were exposed to a local oriented magnetic field based on a tailor-made permanent magnet (0.6 T, Cunying Industrial Co., Ltd., Shanghai, China) for 4 hours a day for 7 consecutive days after injection. The animals were sacrificed by an overdose of anesthesia and cervical dislocation on week 8. The knee joints were dissected, and the surrounding soft tissues were removed carefully without damaging the cartilage.

Gait Analysis

The Catwalk automated gait analysis system (Noldus Information Technology, The Netherlands) was used for the evaluation of joint pain. In brief, each rat walked freely on a glass lit by green lights, and the paw prints were digitized accordingly. The process was recorded with a video camera, and the related data were collected and analyzed using the matching program software (Noldus, CatWalk XT version 10.6.608).

Cartilage Analysis

The samples were fixed in 4% paraformaldehyde for 48 h and then decalcified in 10% EDTA for 6 weeks. The joints were then dehydrated and embedded in paraffin, and sagittally sectioned at 5 μ m thickness. The sections were stained with Prussian blue, safranin-O/fast green (S&F) and hematoxylin-eosin (H&E). S&F staining was used to evaluate the degenerative status of cartilage. The Osteoarthritis Research Society International (OARSI) score was calculated using the following formula: OARSI Score = grade \times stage. H&E staining was used to observe the movement of the tidal line between hyaline cartilage and calcified cartilage. The area of Prussian blue deposition was analyzed using

ImageJ software. The Prussian blue labeling density was calculated using the following equation: (Prussian blue staining area in pixels/total area in pixels) \times 100. For immunochemical evaluation, the sections were incubated with 0.4% pepsin at 37 °C for 1h. Endogenous peroxidase was blocked with 3% H₂O₂, and nonspecific protein binding was blocked with 1% BSA (Sigma). After incubation with primary antibody at 4 °C overnight, the sections were then incubated with the secondary antibody for 30 min at room temperature. The DAB substrate system was used to reveal the color. The levels of circulating cartilage oligomeric matrix protein (COMP) and type II collagen fragments (CTX-II) were measured using ELISA kits. Blood specimens from tail veins were obtained at different time points, and the assays were performed according to the manufacturers' instructions.

Subchondral Bone Analysis

The knee joints were dissected and fixed in 70% ethanol overnight. Samples were scanned using a high-resolution micro-CT system (Skyscan 1172, Germany) and the images were analyzed using data analysis software (CTAn v1.8). The scanner was set at a voltage of 80 kVp, current of 112 μ A and resolution of 15.8 μ m per pixel. Three-dimensional histomorphometric analysis was conducted and the region of interest was defined as the area covering the medial subchondral bone compartment. The parameters analyzed included subchondral bone volume/trabecular volume fraction (BV/TV), trabecular pattern factor (Tb.pf) and trabecular thickness (Tb.Th).

Statistical Analysis

All the values are expressed as the mean \pm standard deviation. Student's *t*-test (two groups), and one-way or two-way analysis of variance (ANOVA, multiple groups), were used for statistical analyses. A *P* value <0.05 was considered to be statistically significant. All data were analyzed using SPSS software (version 22.0, IBM, US).

Results and Discussion

Characterization of KGN-MNPs

After KGN-MNPs were synthesized from MNPs (Figure 1A), electron microscopy images showed that the MNPs and KGN-MNPs had narrow size distribution profiles with average sizes measuring 92.31 and 120.47 nm, respectively (Figure 1B).

To characterize the physicochemical properties, we compared the FTIR spectra of the unmodified MNPs with those of KGN-MNPs (Figure 1C). The MNP-KGN sample showed new spectral peaks at 1532 and 1676 cm^{-1} corresponding to the presence of amide bonds in the molecular structure of KGN. The presence of characteristic polylactide bands at 1187 and 2967 cm^{-1} confirmed the successful conjugation of KGN onto the polylactide-based MNPs. The magnetic properties of MNPs and MNPs-KGN showed that the nanoparticles exhibited typical S-shaped hysteresis curves without remanence, thus demonstrating superparamagnetism. However, the saturation magnetization (*M_s*) of the MNPs-KGN decreased from 66.17 emu/g to 34.03 emu/g due to the nonmagnetic encapsulation layer (Figure 1D). The isoelectric point (pI) values of MNPs and MNPs-KGN nanoparticles (Figure 1E) were identified by measuring the zeta potentials of the nanoparticles in solution as a function of pH. The conjugation of KGN onto the MNPs decreased the pI of the nanoparticle from 6.4 to 4.6, due to an increase in acidic groups on the particle surface. Thermogravimetric analysis (Figure 1F) further showed that the KGN-MNPs had greater than 40% mass loss due to pyrolyzation of the polylactide and KGNs as the temperature increased to 600 °C. In addition, X-ray diffraction analysis (XRD) revealed that the conjugation of KGN did not alter the underlying crystal structures of MNPs (Figure 1G).

Using HPLC, we determined that the KGN encapsulation efficacy was $80.3 \pm 7.5\%$ and that the KGN loading efficacy was $2.4 \pm 0.6\%$. According to the median effective concentration (EC₅₀) of KGN reported as 100 nM,⁵ the concentration of KGN-MNPs was calculated based on the encapsulation and loading efficacy each time to ensure a KGN concentration of 100 nM in the following experiments. Ex vivo release measurements showed that the encapsulated drug was released from KGN-MNPs via first-order kinetics during the initial 10-day period (Figure 1H). The increased sustained release behavior could be attributed to KGN retention in the polylactide matrix, which slowly degraded over time.

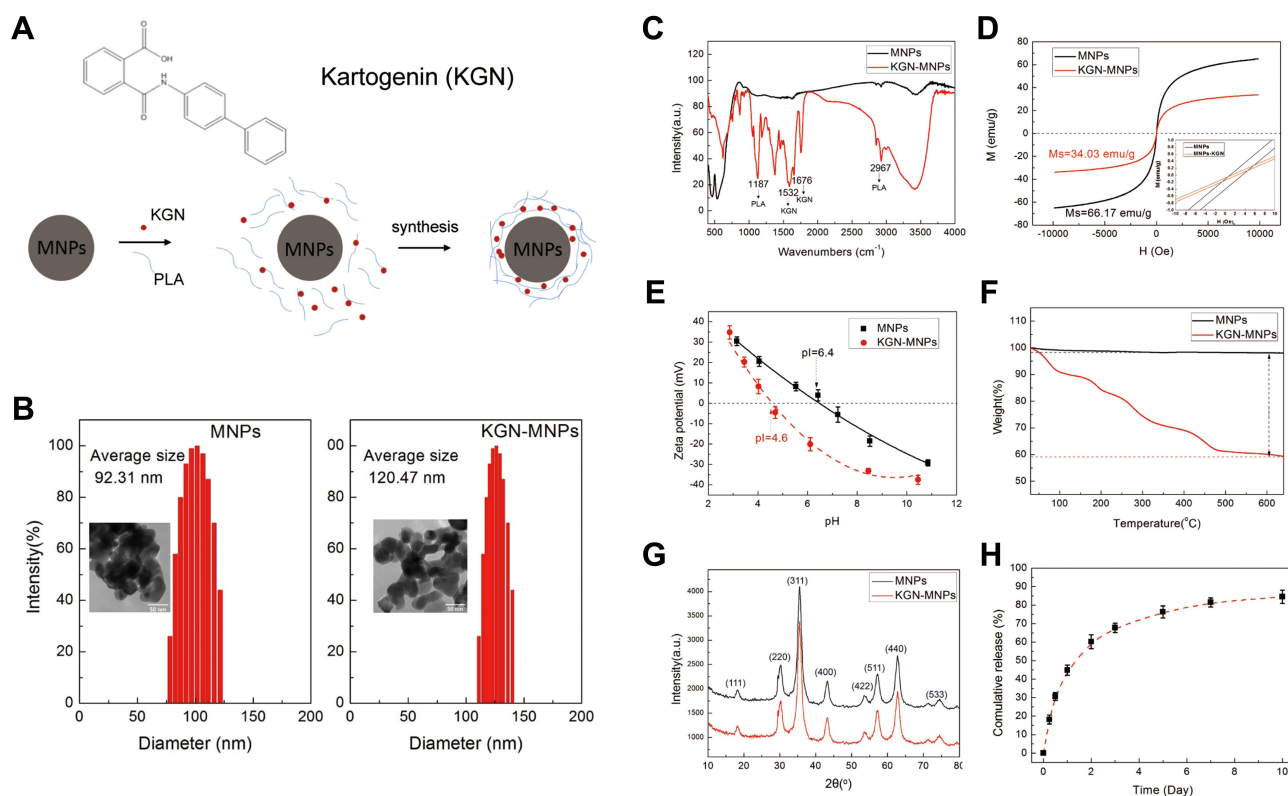


Figure 1 Physiochemical characterization of KGN-MNPs. **(A)** Illustration of the procedures used to synthesize KGN-MNPs. **(B)** Size distributions of agglomerations and TEM images of KGN-MNPs and MNPs. **(C)** FTIR spectra of KGN-MNPs and MNPs. **(D)** The hysteresis loops of KGN-MNPs and MNPs at 25 °C. **(E)** pI value measurements of KGN-MNPs and MNPs. **(F)** Thermogravimetric analysis. **(G)** XRD patterns of KGN-MNPs and MNPs. **(H)** Ex vitro release of KGN from the KGN-MNPs in PBS solution at 37 °C.

Abbreviations: KGN, kartogenin; MNPs, magnetic nanoparticles; KGN-MNPs, KGN loaded MNPs.

KGN-MNPs Induce Chondrogenic Differentiation of MSCs

A schematic illustration and photo of the cell culture protocol are shown in [Figure 2A](#). To investigate the cell uptake of KGN-MNPs by MSCs, we first isolated MSCs from bone marrow and confirmed the internalization of KGN-MNPs in the cells by TEM ([Figure 2B](#)). Next, the cytotoxicity test was performed to evaluate the changes in MSC viability after incubation with different concentrations or types of nanoparticles, in the presence or absence of a magnet. The results indicated no toxicity at KGN-MNP concentrations ≤ 500 $\mu\text{g/mL}$ in the presence or absence of a magnet ([Figure 2C](#)) after 24 h of incubation. The same results were observed after 12, 48 and 72 h of incubation ([Figure 2D](#)). The CCK8 results demonstrated that KGN-loaded MNPs, blank MNPs or the separate components alone were not toxic to the MSCs ([Figure 2E](#)). In addition, the presence of a magnet for the entire incubation duration did not result in a significant change in cell viability.

Cellular accumulation of MNPs was quantified by a ferrozine assay. The results in [Figure 2F](#) illustrated that the uptake of MNPs was both time and concentration dependent. However, we found that PLA modification with KGN caused a minor reduction in MNP uptake compared with a simple mixture of KGN and MNPs, whereas magnets placed underneath the culture plates could significantly enhance the cellular uptake of MNPs by approximately 2.5-fold ([Figure 2G](#)).

To confirm that KGN-MNPs can induce MSC differentiation into chondrocytes, we used a pellet culture system with or without KGN-MNPs. The positive control was the culture system with the addition of TGF- β , which can induce differentiation of MSCs into cartilage tissue.^{30,31} We performed toluidine blue staining on the frozen sections, and the results showed that KGN-MNPs could induce MSCs to form cartilage-like tissue after 21 days of induction, which was consistent with that noted in the positive control group ([Figure 2H](#)).

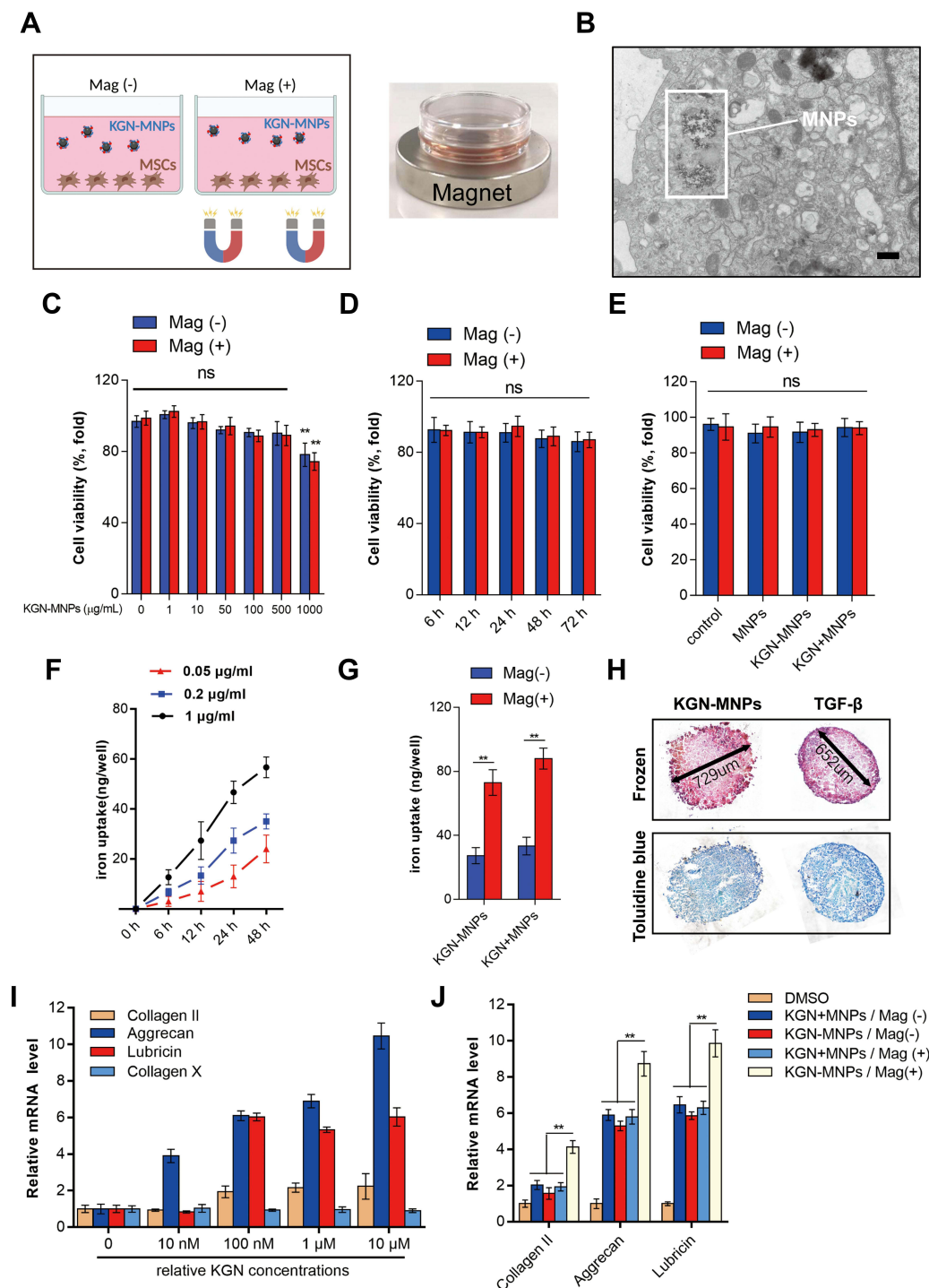


Figure 2 Cellular uptake and cytotoxicity test of KGN-MNPs. **(A)** Schematic illustration and images of the cell culture protocol. **(B)** TEM image of KGN-MNP internalization and encapsulation in MSCs (scale bar= 6 μ m). **(C)** MSC viability after 24 h of incubation with different concentrations of KGN-MNPs. **(D)** No significant changes in cell viability were detected with incubation of KGN-MNPs at different time points with or without a magnet. **(E)** MSC viability after 24 h of incubation with different suspensions showed that none of the tested products were toxic to the cells. **(F)** The cellular uptake of KGN-MNPs was time and concentration dependent. **(G)** Magnet significantly enhanced the cellular uptake of nanoparticles, $**p<0.01$. **(H)** KGN-MNPs induce MSCs into chondrocytes in vitro. **(I)** KGN-MNPs increased chondrocyte-specific gene expression but not Collagen X expression in MSCs. **(J)** Chondrocyte-specific gene expression in MSCs after KGN-MNPs incubation for 72 h with or without the presence of a magnet, $**p<0.01$.

Abbreviations: ns, not significant; KGN, kartogenin; MNPs, magnetic nanoparticles; Mag (+), in the presence of magnet; Mag (-), in the absence of magnet; KGN+MNPs, mixture of KGN and MNPs without reaction; KGN-MNPs, KGN-loaded MNPs.

Next, to confirm the effect of KGN-MNPs on chondrogenesis, the cells were treated with KGN-MNPs as indicated for 72 hours. Type II collagen, aggrecan, and lubricin gene expression was analyzed by real-time polymerase-chain reaction (PCR) as these genes have been previously determined to be upregulated by KGN alone.⁵ The expression of all the genes was normalized to the dimethyl sulfoxide control (DMSO). The results showed that type II collagen, aggrecan, and lubricin gene expression was significantly upregulated in the presence of KGN (Figure 2I). Gene expression in the KGN group was higher than that observed in the KGN-MNP group, which could be attributed to the sustained-release property of KGN-MNPs (approximately 65% at Day 3). However, the group of KGN-MNPs that was subjected to a magnetic field demonstrated the highest gene expression level among all experimental groups, which was probably due to the addition of a magnetic attraction force to the simple sedimentation. Despite exposure to a magnetic field, MNPs not coated with KGN showed no statistically significant difference in gene expression compared to the groups not exposed to a magnet (Figure 2J).

KGN-MNPs Exhibit Improved Penetration Properties

As a proof of concept that our nanoparticles could eventually be used in clinical applications, we tested the efficiency of KGN-MNP persistence in the joint cavity. ACLT was performed on mature male rats which were then used as the OA model. A schematic representation of the experimental steps is shown in Figure 3A. The rats were sacrificed for analysis on week 8.

We then compared nanoparticle penetration with or without the presence of a magnet. Sagittal sections were used to evaluate the depth of MNP penetration based on the existence of Prussian blue stained dots after 8 weeks. In rat cartilage, KGN-MNPs could only be observed within the superficial layer. However, with the presence of oriented magnetic force, KGN-MNPs penetrated a much deeper layer of cartilage, and more positive Prussian blue staining dots could be detected (Figure 3B). The results revealed a remarkable improvement in MNP penetration and an increased amount of MNPs in the presence of a magnet (Figure 3C and Figure 3).

KGN-MNPs Alleviate Inflammation and Protect Against Articular Degeneration

To investigate the protective effect of KGN-MNPs, we extended the observation time to 8 weeks in preclinical OA models. Static paw parameters (print area and light intensity) and dynamic paw parameters (duty cycle, stance phrase, swing phrase and swing speed) were assessed using the CatWalk system to evaluate the efficacy of KGN-MNPs on improving rat movement disability caused by OA. The results of gait analysis (Figure 3E–) further showed that KGN-MNPs improved the duty cycle, print area, stance phrase and swing speed in the animal model. In addition, in the presence of the magnet, KGN-MNPs could further improve other gait-related factors, such as the light intensity and swing phrase at week 8. The results indicated that KGN-MNPs significantly improved rat movement disability caused by OA.

Next, to test cartilage degeneration in the OA models, tissue sections from different groups were stained with S&F (Figure 4A). In the ACLT group, wide areas of cartilage destruction were observed with matrix loss and surface denudation at week 8. In the KGN-MNP group, only a slight protective effect was observed with obvious surface destabilization and thin cartilage. In contrast, in the presence of a local magnetic field, the KGN-MNP group showed generally intact surfaces. In addition, H&E staining showed that the thickness of the calcified cartilage zone in these rats was greater than that with local magnetic exposure with the tidemark moving closer to the articular surface (Figure 4A).

The histologic staining results were consistent with the OARSI scores and Mankins scores. Analysis of the OARSI scores and Mankins scores revealed that the scores were significantly higher in the ACLT group compared with the sham group. KGN treatment did not significantly reduce either OARSI scores or Mankins scores. KGN-MNP treatment significantly decreased both OARSI scores and Mankins scores in OA rats. Moreover, the presence of a magnet further decreased the scores in the KGN-MNP group (Figure 4B and Figure 4). Quantification of OA biomarkers in plasma was also assessed by multiplex ELISA. COMP and CTX-II are well-studied biochemical markers of cartilage and bone turnover and have been reported to be increased in OA.^{32–34} KGN treatment did not significantly alter COMP and CTX-II levels. The KGN-MNP treatment groups showed decreased COMP compared with the OA group, but no significant

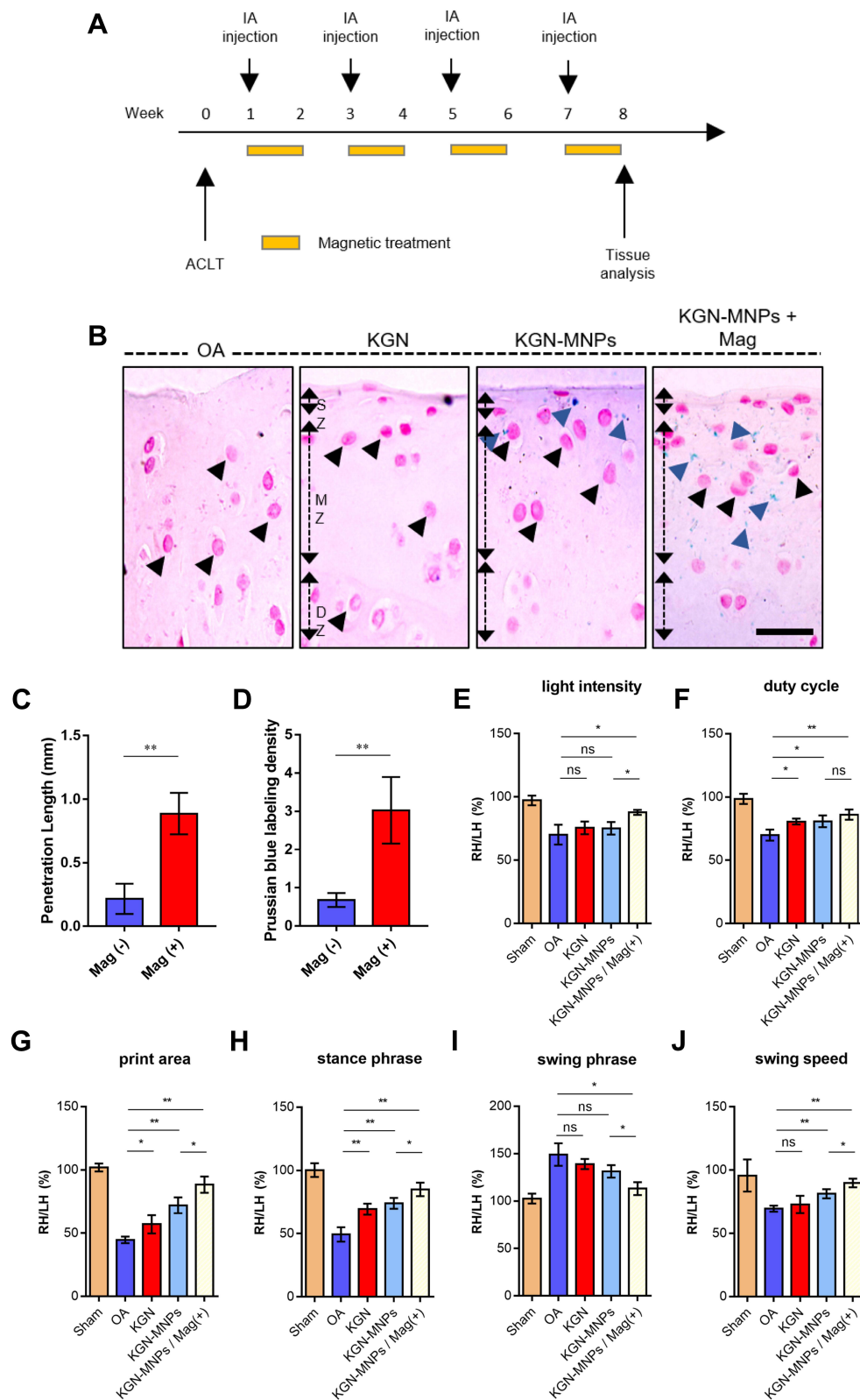


Figure 3 KGN-MNPs exhibit enhanced penetration and show efficacy in improving rat movement disability caused by OA. **(A)** Diagram of in vivo performance. **(B)** KGN-MNPs not exposed to magnets primarily remained in the SZ of cartilage, whereas the application of additional magnetic force increased the penetration into the MZ. Note the enhanced retention ability of the magnet; large amounts of MNPs could be observed in the matrix of the SZ and MZ (scale bar = 200 μ m). **(C)** The magnet could significantly increase the penetration length of KGN-MNPs into the cartilage. **(D)** The magnet significantly increased the amount of KGN-MNPs in the cartilage. **(E–J)** The gaits of rats were analyzed using the Catwalk gait analysis system. * $p < 0.05$, ** $p < 0.01$.

Abbreviations: ns, not significant; KGN, kartogenin; MNPs, magnetic nanoparticles; Mag, magnet; KGN-MNPs, KGN-loaded MNPs.

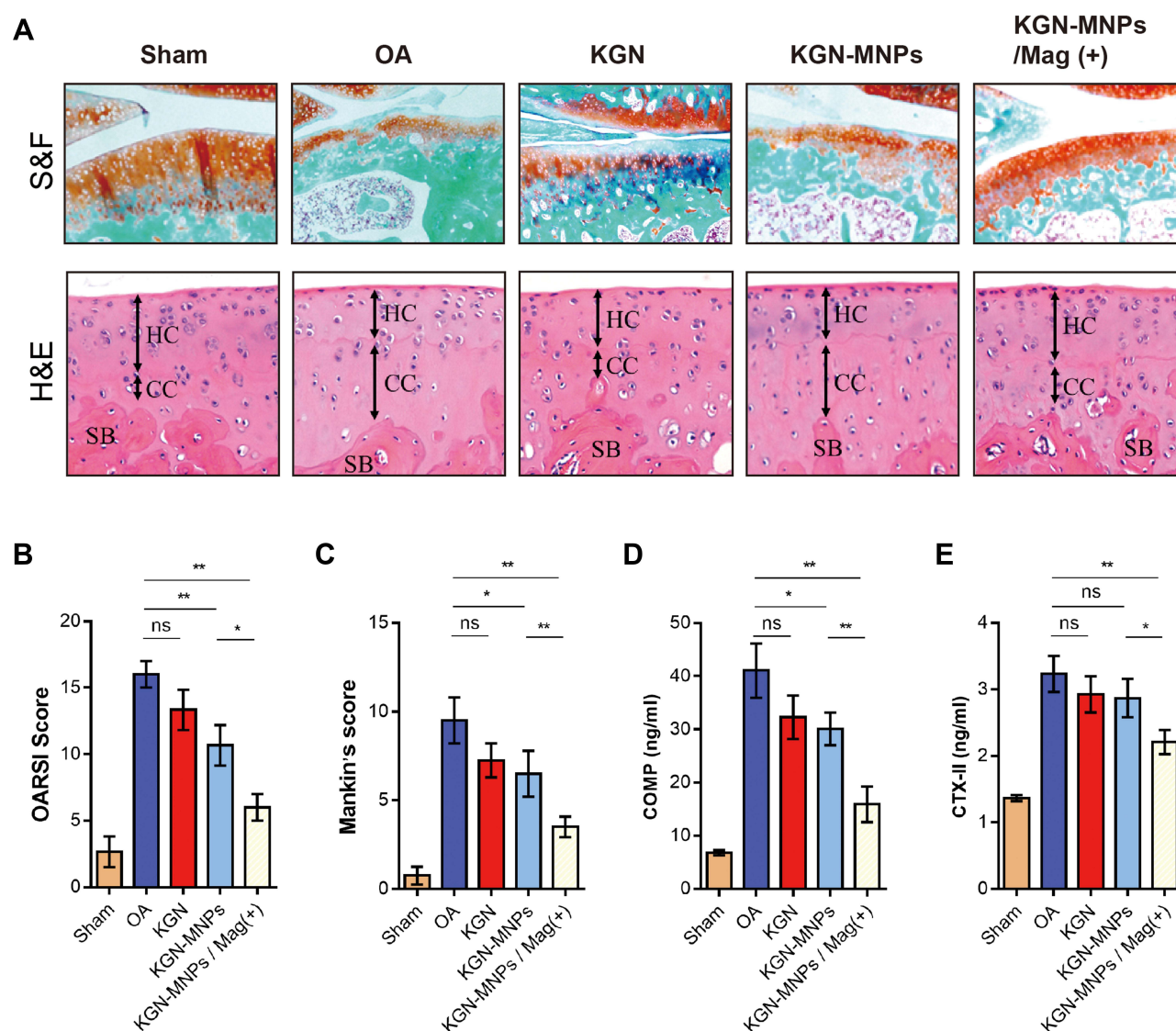


Figure 4 Articular cartilage protection of KGN-MNPs. **(A)** H&E and Safranin O and fast green staining of sagittal sections of the medial tibial plateau. H&E staining showed that KGN-MNPs prevented the upward movement of the tidal line. Proteoglycan (red) and bone (green). (Scale bar= 250 μ m). **(B)** OARSI scores. **(C)** Mankin scores. **(D)** Serum COMP levels. **(E)** Serum CTX-II levels. * $p < 0.05$, ** $p < 0.01$.

Abbreviations: ns, not significant; KGN, kartogenin; MNPs, magnetic nanoparticles; Mag, magnet; KGN-MNPs, KGN-loaded MNPs.

differences in CTX-II levels were found between the OA group and the KGN-MNP group at week 8. Lower COMP and CTX-II levels were noted in the KGN-MNP + Mag group compared with the KGN-MNP group at week 8 (Figure 4D and Figure 4).

KGN-MNPs Reduce Subchondral Bone Defects in OA Models

In addition to the changes in the cartilage, abnormal subchondral bone adaptations were also identified given that cartilage integrity plays an important role in subchondral bone.^{35,36} The structure of medial tibial subchondral bone was analyzed using microCT (Figure 5A and Figure 5). First, compared with the OA group, decreased Tb.pf was observed in the KGN and KGN-MNP treatment groups after 8 weeks. Notably, compared with the KGN-MNP groups, the additional presence of a magnetic field displayed reduced BV/TV and Tb.pf, and increased Tb.Th with significant differences, indicating that KGN-MNPs with additional magnetic force had a better protective effect on subchondral bones (Figure 5C–).

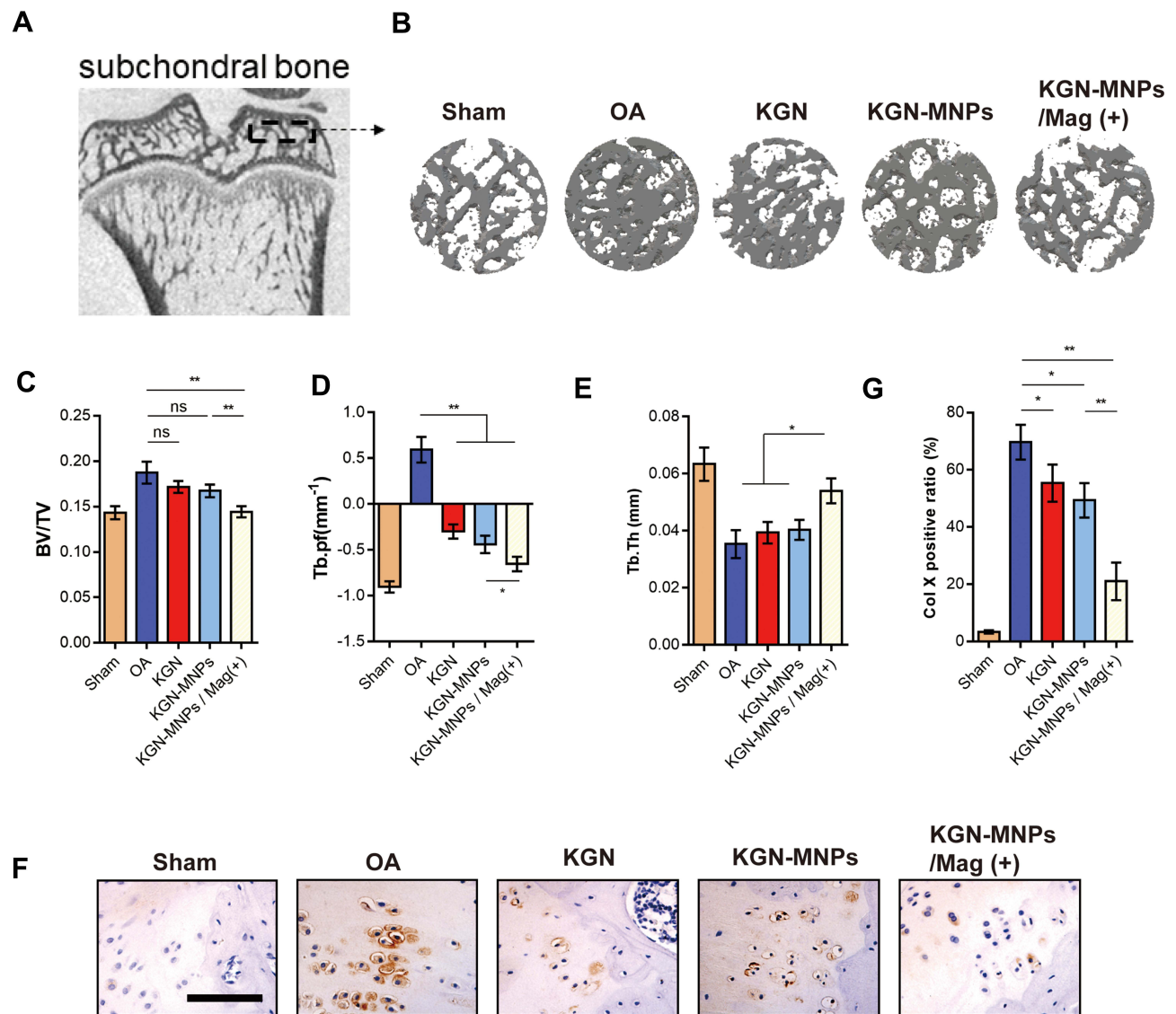


Figure 5 KGN-MNPs normalize subchondral bone after anterior cruciate ligament transection. (**A** and **B**) Representative micro-CT images of longitudinal views of subchondral bone medial compartment. (Scale bar= 500 μ m). Quantitative micro-CT analysis of tibial subchondral bone of BV/TV (**C**), Tb.pf (**D**), and Tb.th (**E**). Immunohistochemical (**F**) and quantitative (**G**) analyses of type X collagen in the calcified cartilage. (Scale bar= 100 μ m). * p <0.05, ** p <0.01.

Abbreviations: ns, not significant; KGN, kartogenin; MNPs, magnetic nanoparticles; Mag, magnet; KGN-MNPs, KGN-loaded MNPs.

Furthermore, we observed a clear immune reactivity of type X collagen (Col X) in the calcified cartilage zone surrounding the hypertrophic chondrocytes in the OA group (Figure 5F). Of note, although KGN does not affect type X collagen expression (hypertrophy-related gene of chondrocytes) according to our in vitro study results (Figure 2G) and a previous report,⁵ KGN-MNPs in the context of a magnet could obviously reduce the expression of Col X and showed statistically significant differences relative to either group (Figure 5G). This finding could be due to the deep penetration of KGN-MNPs in the context of additional magnetic force.

Interactions between cells and nanosized polymeric carriers have been reported for many types of cells such as cancer cells, endothelial cells, and immunocytes.^{37–39} However, studies regarding MSC interactions with MNPs are limited. In this study, we sought to enhance the biological function of MSCs with nanoparticles. From our assessment, MNPs coated with KGN promoted the selective differentiation of MSCs into chondrocytes. Moreover, the presence of a local magnet effectively strengthened the uptake of MNPs, which ultimately led to the increased accumulation of KGN in the MSCs. Our results showed that KGN-MNPs with an additional magnetic field could increase the expression of gene products associated with chondrocytes compared with other KGN groups.

In the knee joint, several tissues, including bone marrow, synovial membrane and adipose tissue, can generate MSCs, which have the capacity for chondrogenesis and cartilage self-repair. Articular cartilage is a physiologically avascular tissue with a singular cell type (chondrocyte) that was once believed to be lacking in intrinsic reparative ability given the lack of MSCs. Recent studies demonstrate that articular cartilage contains a population of stem/progenitor cells that are potentially involved in the maintenance of tissue homeostasis. These cartilage-derived stem/progenitor cells have been identified and exhibit clonogenicity, multipotency, and migratory activity.^{40,41} Previous studies reported that KGN promoted the differentiation of MSCs into chondrocytes and showed chondro-protective effects.^{5,42} These findings support our strategy of using a local magnetic field to trigger a more pronounced retention and internalization of KGN in MSCs with our drug delivery system.

Intra-articular drug delivery administration does not guarantee persistent drug retention or sufficient drug penetration into cartilage tissue to elicit the desired biological response. Here, we provide our perspective on the utilization of MNPs to prevent the rapid loss of drug to the lymphatics and capillaries, and to enhance drug penetration and transport into cartilage upon the application of additional magnetic force. Our study indicated that KGN-MNP treatment with an external magnetic force had better outcomes with less cartilage degeneration, fewer subchondral bone changes, and a longer injection interval.

Toxic Effects of KGN-MNPs on Organisms

Histological analysis of the visceral organs (heart, liver, spleen, lung and kidney) stained with H&E was performed to evaluate the potential biotoxicity of KGN-MNPs. No obvious pathological changes, such as inflammatory cell infiltration or tissue necrosis, were observed, supporting the future clinical use of KGN-MNPs in humans (Figure 6A). Histological analysis of the knee joint synovium was also performed to investigate whether KGN-MNPs would lead to synovial

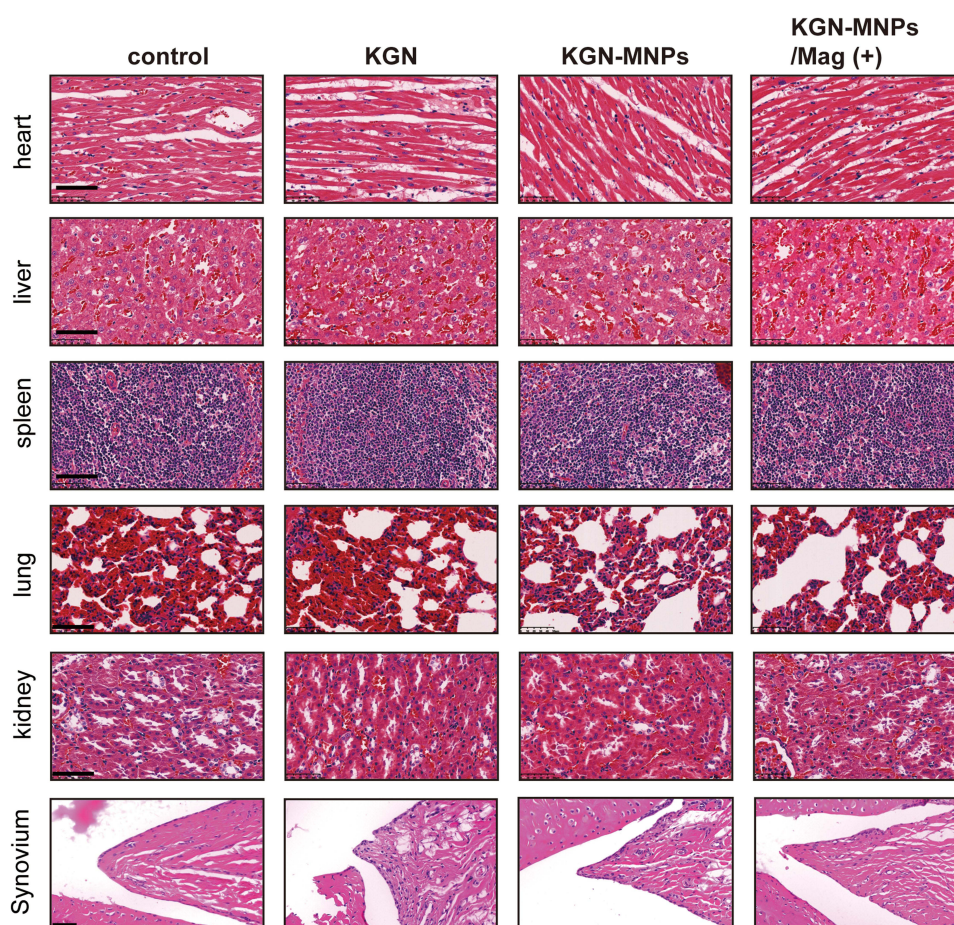


Figure 6 Histological analyses of major organs and synovial tissues. No obvious pathological changes were observed in the lungs, heart, liver, spleen, kidneys or synovial tissues of rats treated with KGN-MNPs with or without magnets, indicating that KGN-MNPs did not lead to significant organ and joint toxicity at 8 weeks.

Abbreviations: KGN, kartogenin; MNPs, magnetic nanoparticles; KGN-MNPs, KGN loaded MNPs; Mag, magnet.

inflammation (Figure 4A). Compared with the control groups, KGN-MNP treatment did not cause obvious pathological changes in the synovium at week 8 with or without magnets (Figure 6B).

Conclusions

In summary, we demonstrated the use of PLA-coated iron oxide nanoparticles as a delivery system for KGN in OA treatment. We found that the application of MNPs and an external magnetic field apparently increased KGN retention in MSCs, promoted the penetration of more KGN-MNPs into cartilage, avoided the rapid clearance of KGN in joints, and enhanced the utilization of KGN. Our study provides evidence confirming the feasibility and effectiveness of magnetic nanoparticles for stem cell-based therapy for OA treatment, which holds great promise for clinical translation. In future experiments, local magnetic forces will be regulated to change the entry depth of nanoparticles, and larger animals, such as rabbits and monkeys, will be utilized for assessments of pharmacokinetics, safety, and efficacy.

Ethics Approval and Consent to Participate

All the animal procedures were approved by Institutional Animal Care and Use Committee of Shanghai Sixth People's Hospital (No. 2021-0194) in accordance with the guidelines of the Chinese Society of Laboratory Animals on animal welfare.

Author Contributions

All authors made a significant contribution to the work reported, whether that is in the conception, study design, execution, acquisition of data, analysis and interpretation, or in all these areas; took part in drafting, revising or critically reviewing the article; gave final approval of the version to be published; have agreed on the journal to which the article has been submitted; and agree to be accountable for all aspects of the work.

Funding

This study was supported in part by the National Nature Science Foundation of China (81702133), and Excellent Youth Training Program of Shanghai Jiaotong University Affiliated Sixth People's Hospital (ynyq202102).

Disclosure

The authors declare no competing financial interest.

References

1. Hunter DJ, Bierma-Zeinstra S. Osteoarthritis. *Lancet*. 2019;393(10182):1745–1759. doi:10.1016/S0140-6736(19)30417-9
2. Bijlsma JW, Berenbaum F, Lafeber FP. Osteoarthritis: an update with relevance for clinical practice. *Lancet*. 2011;377(9783):2115–2126. doi:10.1016/S0140-6736(11)60243-2
3. Fahy N, Alini M, Stoddart MJ. Mechanical stimulation of mesenchymal stem cells: implications for cartilage tissue engineering. *J Orthop Res*. 2018;36(1):52–63. doi:10.1002/jor.23670
4. Ma Q, Liao J, Cai X. Different sources of stem cells and their application in cartilage tissue engineering. *Curr Stem Cell Res Ther*. 2018;13(7):568–575.
5. Johnson K, Zhu S, Tremblay MS, et al. A stem cell-based approach to cartilage repair. *Science*. 2012;336(6082):717–721.
6. Rai MF, Pham CT. Intra-articular drug delivery systems for joint diseases. *Curr Opin Pharmacol*. 2018;40:67–73.
7. Riggall CN, Tucker JJ, Soslowsky LJ, Kuntz AF. Intra-articular tibiofemoral injection of a nonsteroidal anti-inflammatory drug has no detrimental effects on joint mechanics in a rat model. *J Orthop Res*. 2014;32(11):1512–1519.
8. Jones IA, Togashi R, Wilson ML, Heckmann N, Vangsness CT Jr. Intra-articular treatment options for knee osteoarthritis. *Nat Rev Rheumatol*. 2019;15(2):77–90.
9. Evans CH, Ghivizzani SC, Robbins PD. Gene delivery to joints by intra-articular injection. *Hum Gene Ther*. 2018;29(1):2–14.
10. Xiao L, Cui J, Sun Z, Liu Y, Zheng J, Dong Y. Therapeutic potential of nanotechnology-based approaches in osteoarthritis. *Front Pharmacol*. 2022;13:920824. doi:10.3389/fphar.2022.920824
11. Ma L, Zheng X, Lin R, et al. Knee osteoarthritis therapy: recent advances in intra-articular drug delivery systems. *Drug Des Devel Ther*. 2022;16:1311–1347. doi:10.2147/DDDT.S357386
12. Bajpayee AG, Grodzinsky AJ. Cartilage-targeting drug delivery: can electrostatic interactions help? *Nat Rev Rheumatol*. 2017;13(3):183–193. doi:10.1038/nrrheum.2016.210
13. Tryfonidou MA, de Vries G, Hennink WE, Creemers LB. "Old Drugs, New Tricks" - Local controlled drug release systems for treatment of degenerative joint disease. *Adv Drug Deliv Rev*. 2020;160:170–185. doi:10.1016/j.addr.2020.10.012

14. Mohammadinejad R, Ashrafzadeh M, Pardakhty A, et al. Nanotechnological strategies for osteoarthritis diagnosis, monitoring, clinical management, and regenerative medicine: recent advances and future opportunities. *Curr Rheumatol Rep.* 2020;22(4):12. doi:10.1007/s11926-020-0884-z
15. Mancipe Castro LM, Garcia AJ, Guldberg RE. Biomaterial strategies for improved intra-articular drug delivery. *J Biomed Mater Res A.* 2021;109(4):426–436. doi:10.1002/jbm.a.37074
16. Dash S, Das T, Patel P, Panda PK, Suar M, Verma SK. Emerging trends in the nanomedicine applications of functionalized magnetic nanoparticles as novel therapies for acute and chronic diseases. *J Nanobiotechnology.* 2022;20(1):393. doi:10.1186/s12951-022-01595-3
17. Mokhosi SR, Mdilalose W, Nhlalo A, Singh M. Advances in the synthesis and application of magnetic ferrite nanoparticles for cancer therapy. *Pharmaceutics.* 2022;14:5. doi:10.3390/pharmaceutics14050937
18. Wang R, Degirmenci V, Xin H, et al. PEI-Coated Fe₃O₄ nanoparticles enable efficient delivery of therapeutic siRNA targeting REST into glioblastoma cells. *Int J Mol Sci.* 2018;19(8):10.
19. Martinkova P, Brtnicky M, Kynicky J, Pohanka M. Iron oxide nanoparticles: innovative tool in cancer diagnosis and therapy. *Adv Healthcare Mater.* 2018;7:5. doi:10.1002/adhm.201700932
20. Halder J, Pradhan D, Biswasroy P, et al. Trends in iron oxide nanoparticles: a nano-platform for theranostic application in breast cancer. *J Drug Target.* 2022. 1–21. doi:10.1080/1061186X.2022.2095389
21. Kiru L, Zlitni A, Tousley AM, et al. In vivo imaging of nanoparticle-labeled CAR T cells. *Proc Natl Acad Sci U S A.* 2022;119(6). doi:10.1073/pnas.2102363119
22. Sambhudevan SH, Sambhudevan S. Ferrite-based polymer nanocomposites as shielding materials: a review. *Chemical Papers.* 2021;75(8):3697–3710. doi:10.1007/s11696-021-01664-1
23. Singhvi MS, Zinjarde SS, Gokhale DV. Polylactic acid: synthesis and biomedical applications. *J Appl Microbiol.* 2019;127(6):1612–1626. doi:10.1111/jam.14290
24. Darwish MSA, Nguyen NHA, Ševců A, Stibor I. Functionalized magnetic nanoparticles and their effect on Escherichia coli and Staphylococcus aureus. *J Nanomater.* 2015;2015:1–10. doi:10.1155/2015/416012
25. Beagan AM, Alghamdi AA, Lahmadi SS, et al. Folic acid-terminated poly(2-diethyl amino ethyl methacrylate) brush-gated magnetic mesoporous nanoparticles as a smart drug delivery system. *Polymers.* 2020;13:1. doi:10.3390/polym13010059
26. Baker N, Boyette LB, Tuan RS. Characterization of bone marrow-derived mesenchymal stem cells in aging. *Bone.* 2015;70:37–47. doi:10.1016/j.bone.2014.10.014
27. Ding N, Li E, Ouyang X, Guo J, Wei B. The therapeutic potential of bone marrow mesenchymal stem cells for articular cartilage regeneration in osteoarthritis. *Curr Stem Cell Res Ther.* 2021;16(7):840–847. doi:10.2174/1574888X16666210127130044
28. Zhen G, Wen C, Jia X, et al. Inhibition of TGF- β signaling in mesenchymal stem cells of subchondral bone attenuates osteoarthritis. *Nat Med.* 2013;19(6):704–712. doi:10.1038/nm.3143
29. Zhen G, Guo Q, Li Y, et al. Mechanical stress determines the configuration of TGF β activation in articular cartilage. *Nat Commun.* 2021;12(1):1706. doi:10.1038/s41467-021-21948-0
30. Mishra PJ, Banerjee D. Activation and Differentiation of Mesenchymal Stem Cells. *Method Mol Biol.* 2017;1554:201–209.
31. Crane JL, Cao X. Bone marrow mesenchymal stem cells and TGF- β signaling in bone remodeling. *J Clin Invest.* 2014;124(2):466–472. doi:10.1172/JCI70050
32. Fu Y, Huang Y, Yang Z, et al. Cartilage oligomeric matrix protein is an endogenous β -arrestin-2-selective allosteric modulator of AT1 receptor counteracting vascular injury. *Cell Res.* 2021;31(7):773–790.
33. Hao HQ, Zhang JF, He QQ, Wang Z. Cartilage oligomeric matrix protein, C-terminal cross-linking telopeptide of type II collagen, and matrix metalloproteinase-3 as biomarkers for knee and Hip osteoarthritis (OA) diagnosis: a systematic review and meta-analysis. *Osteoarthritis Cartilage.* 2019;27(5):726–736.
34. Posey KL, Coustry F, Hecht JT. Cartilage oligomeric matrix protein: cOMPopathies and beyond. *Matrix Biol.* 2018;71:161–173.
35. Mahjoub M, Berenbaum F, Houard X. Why subchondral bone in osteoarthritis? The importance of the cartilage bone interface in osteoarthritis. *Osteoporos Int.* 2012;23(Suppl 8):S841–846.
36. Hu Y, Chen X, Wang S, Jing Y, Su J. Subchondral bone microenvironment in osteoarthritis and pain. *Bone Res.* 2021;9(1):20.
37. Kim SE, Zhang L, Ma K, et al. Ultrasmall nanoparticles induce ferroptosis in nutrient-deprived cancer cells and suppress tumour growth. *Nat Nanotechnol.* 2016;11(11):977–985.
38. Huang C, Yang G, Ha Q, Meng J. Multifunctional WS. "smart" particles engineered from live immunocytes: toward capture and release of cancer cells. *Adv Mater.* 2015;27(2):310–313.
39. Tay CY, Setyawati MI, Leong DT. Nanoparticle density: a critical biophysical regulator of endothelial permeability. *ACS Nano.* 2017;11(3):2764–2772.
40. Chagin AS, Medvedeva EV. Regenerative medicine: cartilage stem cells identified, but can they heal? *Nat Rev Rheumatol.* 2017;13(9):522–524.
41. Jiang Y, Tuan RS. Origin and function of cartilage stem/progenitor cells in osteoarthritis. *Nat Rev Rheumatol.* 2015;11(4):206–212.
42. Ren E, Chen H, Qin Z, et al. Harnessing bifunctional ferritin with kartogenin loading for mesenchymal stem cell capture and enhancing chondrogenesis in cartilage regeneration. *Adv Healthcare Mater.* 2022;11(8):e2101715.